Chemical Science

ROYAL SOCIETY OF CHEMISTRY

EDGE ARTICLE

View Article Online
View Journal | View Issue

Cite this: *Chem. Sci.*, 2023, **14**, 5014

All publication charges for this article have been paid for by the Royal Society of Chemistry

Origin of intersystem crossing in highly distorted organic molecules: a case study with red light-absorbing *N,N,O,O*-boron-chelated Bodipys†

Xue Zhang, ‡[a] Andrey A. Sukhanov, ‡[b] Xi Liu,‡[c] Maria Taddei,[d] Jianzhang Zhao, *[a] Anthony Harriman, *[e] Violeta K. Voronkova, *[b] Yan Wan, *[c] Bernhard Dick *[f] and Mariangela Di Donato *[dg]

Received 15th February 2023
Accepted 14th April 2023

DOI: 10.1039/d3sc00854a

rsc.li/chemical-science

To explore the relationship between the twisted π-conjugation framework of aromatic chromophores and the efficacy of intersystem crossing (ISC), we have studied a *N,N,O,O*-boron-chelated Bodipy derivative possessing a severely distorted molecular structure. Surprisingly, this chromophore is highly fluorescent, showing inefficient ISC (singlet oxygen quantum yield, $\Phi_\Delta = 12\%$). These features differ from those of helical aromatic hydrocarbons, where the twisted framework promotes ISC. We attribute the inefficient ISC to a large singlet-triplet energy gap ($\Delta E_{S_1/T_1} = 0.61$ eV). This postulate is tested by critical examination of a distorted Bodipy having an anthryl unit at the *meso*-position, for which Φ_Δ is increased to 40%. The improved ISC yield is rationalized by the presence of a T_2 state, localized on the anthryl unit, with energy close to that of the S_1 state. The electron spin polarization phase pattern of the triplet state is (*e*, *e*, *e*, *a*, *a*, *a*), with the T_z sublevel of the T_1 state overpopulated. The small zero-field splitting *D* parameter (−1470 MHz) indicates that the electron spin density is delocalized over the twisted framework. It is concluded that twisting of π-conjugation framework does not necessarily induce ISC, but S_1/T_n energy matching may be a generic feature for increasing ISC for a new-generation of heavy atom-free triplet photosensitizers.

Introduction

Triplet photosensitizers (PSs) should possess significant absorption in the visible or near-UV region, efficient intersystem crossing (ISC), and reversible electrochemistry with well-defined redox potentials.[1–3] Such compounds are crucial for the development of photocatalytic cycles,[4–7] including solar fuel formation *via* water splitting[8–12] or fixation of CO_2,[13–15] photodynamic therapy,[1,16–21] and triplet-triplet-annihilation upconversion.[22–25] However, ISC is a spin forbidden process, being largely ineffective for organic compounds with extended planar π-conjugation frameworks.[26] Spin orbit coupling (SOC) usually vanishes for these compounds due to the planar molecular structure,[27] while a large energy gap between S_1 and T_1 states is also a common feature. These two factors combine to minimize ISC rates. An additional factor that inhibits ISC in aromatic compounds is the large electronic exchange energy for the frontier molecular orbitals, which increases the S_1/T_1 energy gap. In addition, the planarity and high symmetry of the π-conjugation systems serve to reduce the SOC matrix element (SOCME).[26,28] These various parameters influence the rate constant for ISC in accordance with the Fermi Golden rule (eqn (1)):

$$k_{ISC} = \frac{2\pi}{\hbar}\left\langle S_n \middle| \hat{H}_{SO} \middle| T_m \right\rangle^2 \times [\mathrm{FCWD}] \quad (1)$$

[a]*State Key Laboratory of Fine Chemicals, Frontiers Science Center for Smart Materials, School of Chemical Engineering, Dalian University of Technology, Dalian 116024, P. R. China. E-mail: zhaojzh@dlut.edu.cn*

[b]*Zavoisky Physical-Technical Institute, FRC Kazan Scientific Center of Russian Academy of Sciences, Kazan 420029, Russia. E-mail: vio@kfti.knc.ru*

[c]*College of Chemistry, Beijing Normal University, Beijing 100875, P. R. China. E-mail: wanyan@bnu.edu.cn*

[d]*LENS (European Laboratory for Non-Linear Spectroscopy), Via N. Carrara 1, 50019 Sesto Fiorentino (FI), Italy. E-mail: didonato@lens.unifi.it*

[e]*Molecular Photonics Laboratory, School of Natural and Environmental Sciences, Newcastle University, Newcastle Upon Tyne, NE1 7RU, UK. E-mail: anthony.harriman@newcastle.ac.uk*

[f]*Lehrstuhl für Physikalische Chemie, Institut für Physikalische und Theoretische Chemie, Universität Regensburg, D-93053 Regensburg, Germany. E-mail: Bernhard.Dick@chemie.uni-regensburg.de*

[g]*ICCOM, Istituto di Chimica dei Complessi OrganoMetallici, Via Madonna del Piano 10, 50019 Sesto Fiorentino (FI), Italy*

† Electronic supplementary information (ESI) available: General experimental methods, synthesis of compounds, molecular structure characterization, X-ray crystallographic data, computational details and additional spectra. CCDC 2210911. For ESI and crystallographic data in CIF or other electronic format see DOI: https://doi.org/10.1039/d3sc00854a

‡ These authors contributed equally to this work.

where $\hbar$ is the reduced Planck constant, [FCWD] is the Franck–Condon weighted density of states, which usually decays exponentially with the S_n/T_m energy gap. Certain structural motifs can be introduced to enhance ISC in organic compounds. The spin orbit coupling is increased by the presence of heavy atoms (*e.g.*, Ir, Pt, Ru, Br, I, or Se *etc.*)[20,29–33] attached to the π-conjugation framework. Another approach involves mixing n–π* ↔ π–π* transitions according to El Sayed's rule.[26,34,35] Excitonic coupling effects within molecular dimers, with specific mutual orientation of the two chromophores, can also lead to increased ISC.[36–38] Electron spin converters, such as C_{60}, have been used to prepare heavy atom-free triplet PSs.[19,39–44] Similar effects can be obtained using stable free-radicals.[45–47] Recently, charge recombination in orthogonal electron donor–acceptor dyads has been shown to promote ISC (*via* the so-called spin–orbit charge transfer ISC, SOCT-ISC).[48,49] There are, however, drawbacks to each of these protocols, such as the challenging synthesis of complicated molecular structures, cost, toxicity, and chemical stability.[2,3,17,50] It is clear that new ISC mechanisms without the above mentioned limitations are needed.[2,3,17,50,51]

Within this context, we note that ISC induced by a helical π-conjugation structure might offer new perspectives.[27,28,52–58] It is known that for helicenes, ISC is due to the non-vanishing SOCMEs at each molecular orbital component.[27] However, helicenes are not ideal triplet PSs because of their poor visible light absorption, and their challenging derivatization.[59,60] Recently, twisted π-conjugation framework-induced ISC was observed for certain chromophores, including perylenebisimide (PBI).[28,52–54] We and other groups also found that twisted Bodipy derivatives show efficient ISC, as for instance, the naphtha[*b*]-fused Bodipy (triplet state quantum yield, $\Phi_T = 52\%$)[58] and the dihydronaphto[*a*]-fused Bodipy (singlet oxygen quantum yield, $\Phi_\Delta = 55\%$).[53,55,61] Moreover, the electron spin selectivity of the ISC process, manifested by the electron spin polarization (ESP) phase pattern of the triplet state, is highly dependent on molecular structure.[55,58,61,62] Intriguingly, twisted Bodipy structures do not always give efficient ISC, in marked contrast to the helicenes,[57] and recent work by Vennapusa reports the same situation with PBI.[63]

In seeking to expand the range of structurally distorted chromophores absorbing in the red region, our attention has returned to the helical *N*,*N*,*O*,*O* boron-chelated dipyrromethenes (**BO**).[64,65] The synthesis of such compounds is relatively straightforward and there remains the strong possibility that the twisted geometry will promote triplet formation.[27,66] Although the helical structure was introduced as a mean to enhance fluorescence of the 3,5-arylated Bodipy derivatives,[64] the fluorescence quantum yields are lower than those of the native Bodipy. Coordination of two 3,5-*ortho*-phenolic substituents to the central boron atom reduces the molecular symmetry and enforces helicity, thereby leading to circularly polarized luminescence.[65] The same synthetic approach can be applied to develop near-IR absorbing compounds,[67–71] and to construct supramolecular assemblies.[72] To the best of our knowledge, however, the ISC characteristics of these compounds have not been investigated. Now, using a variety of time-resolved spectroscopic tools, together with quantum chemical calculations, we compare the photophysical properties of a *N*,*N*,*O*,*O*-boron-chelated Bodipy (**Ph-BO**) possessing a severely twisted π-conjugation framework with those of the corresponding compound bearing an anthryl moiety at the *meso*-position of the dipyrrin core (**An-BO**). This latter functionalization adds an additional triplet level (T_2) to the excited state manifold which turns out to be crucial in terms of the propensity for ISC.

Results and discussion

Molecular structure design and synthesis

Initial studies focus on determination of the photophysical properties of a known compound, **Ph-BO** (Scheme 1),[65] for

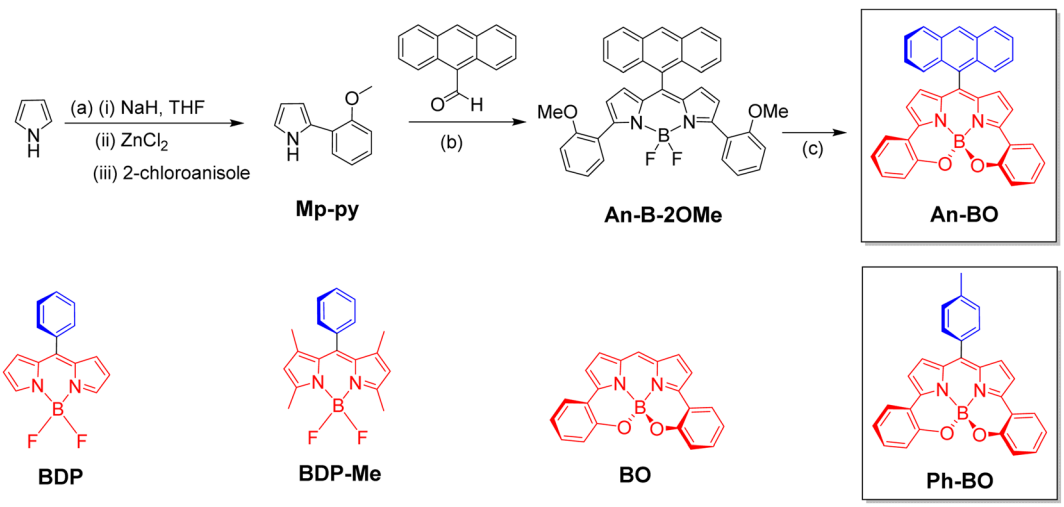

Scheme 1 Synthetic scheme for preparation of **An-BO**. The molecular formulae of the reference compounds are also presented, **BO** is a reference compound used in the computational work. (a) (i) NaH, THF, (ii) $ZnCl_2$, (iii) $Pd(OAc)_2$, JohnPhos, 2-chloroanisole, reflux, 24 h, yield: 49%.[73,74] (b) 9-Anthraldehyde, trifluoroacetic acid, rt, 2 h, reflux, overnight; then DDQ, reflux, overnight; then triethylamine, 30 min, $BF_3{\cdot}Et_2O$, reflux, 4 h, THF, overall yield: 21%.[75] (c) BBr_3, DCM, yield: 49%.[65]

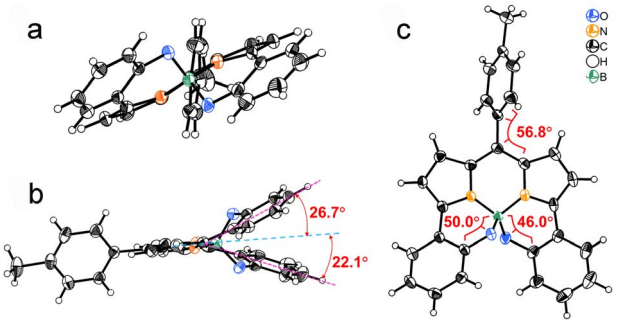

Fig. 1 ORTEP views of the molecular structure determined by single-crystal X-ray diffraction of **Ph-BO**. (a) Bottom view, (b) side view and (c) front view. The dihedral angle between the *meso*-phenyl and dipyrrin moieties and the twist angle are highlighted. Thermal ellipsoids are at 50% probability. CCDC number: 2 210 911 contains detailed information for **Ph-BO**.

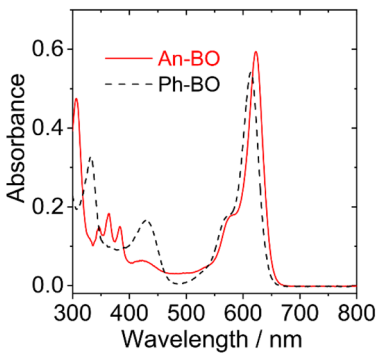

Fig. 2 UV/vis absorption spectra recorded for **An-BO** and **Ph-BO** in acetonitrile. $c = 1.0 \times 10^{-5}$ M, 25 °C.

which we find the rather modest triplet yield of *ca.* 12%. Two strategies can be invoked when seeking to increase triplet quantum yield, SOCT-ISC[51,76–78] and minimizing the singlet-triplet energy gap by introducing an intermediate triplet state localized on a *meso*-substituent. Both concepts can be examined using a *meso*-anthryl derivative, **An-BO**.[79,80] Synthesis of the latter is based on the known derivatization of this kind of twisted Bodipy derivative. The yield was judged to be satisfactory and the molecular structure has been verified by ^{1}H NMR, ^{13}C NMR and HR MS spectroscopic methods (for details, see the ESI†).

Single crystals of **Ph-BO** were obtained by slow diffusion of *n*-hexane (HEX) into a dichloromethane (DCM) solution. Subsequent X-ray diffraction studies show that the angle between the planes defined by the two pyrrolic rings is 48.8°.

The two phenyl rings deviate from the mean plane of the dipyrrin by *ca.* 22.1° and 26.7°, confirming that the molecular structure is highly twisted (Fig. 1b). The O–B–O, N–B–N and O–B–N bond angles are 107.6°, 105.6°, 106.8°, respectively (Fig. 1c). These data show a distorted tetrahedral boron center, while angles are similar to those of previously reported analogues.[64,81]

Steady-state optical spectra

The UV/vis absorption spectra recorded for **An-BO** and **Ph-BO** are shown in Fig. 2. Both compounds exhibit a strong absorption band at *ca.* 620 nm, the molar absorption coefficient for **An-BO**, $\varepsilon = 59\,000$ M^{-1} cm^{-1}, being somewhat more pronounced than the previously reported *N*,*N*,*O*,*O*-boron-chelated Bodipy analogue ($\varepsilon = 46\,000$ M^{-1} cm^{-1}).[64] The red-shifted absorption of the helical derivatives compared to the corresponding precursor indicates an expanded π-conjugation system.[64,67] For **An-BO**, an additional structured absorption band was observed in the range of 330–400 nm, attributed to the anthryl moiety, indicating only minor electronic interaction between the anthracene substituent and the dipyrrin core at the ground state.[83]

The corresponding fluorescence spectra are presented in Fig. 3. **Ph-BO** has a strong emission band (fluorescence quantum yield, $\Phi_F = 73\%$, Table 1), whose position and intensity are independent of solvent polarity (Fig. 3c). The strong fluorescence is noteworthy because ISC is usually efficient for helicenes. Recent results from our laboratory,[55–58] and Hasobe's laboratory[53] show that twisted Bodipys can also display efficient ISC. A similar fluorescence spectrum is observed for **An-BO** (Fig. 3b), although the fluorescence quantum yield is lower ($\Phi_F = 48\%$, Table 1). Furthermore, no charge-transfer emission band could be observed for **An-BO**, the fluorescence emission intensity and wavelength do not change with solvent polarity, these properties are uncommon compared to previously reported anthryl-Bodipy dyads.[48,62,84] The singlet state energy (E_{00}) of the compounds, determined as the crossover point of

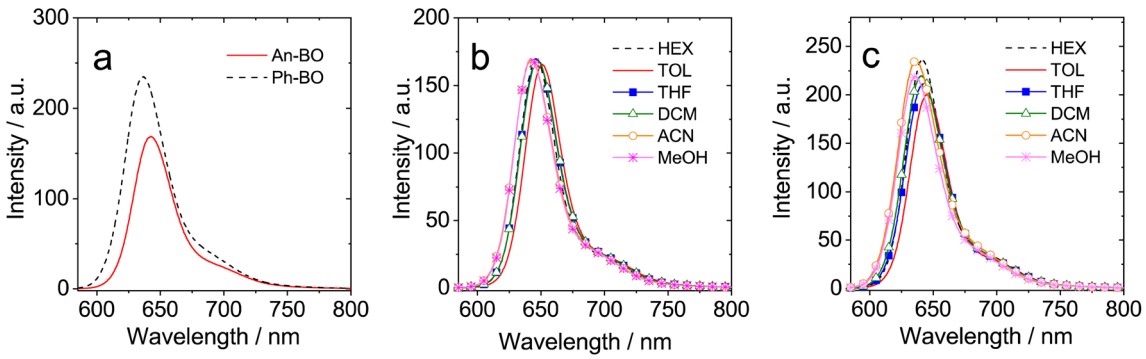

Fig. 3 Fluorescence spectra of (a) **An-BO** and **Ph-BO** in acetonitrile, (b) **An-BO** and (c) **Ph-BO** in different solvents. Optically matched solutions were used in each panel (each of the solutions gives the same absorbance at the excitation wavelength, $A = 0.100$), $\lambda_{ex} = 580$ nm, 25 °C.

Table 1 Photophysical parameters of the compounds[a]

Compounds	λ_{abs}[b] [nm]	ε[c]	λ_{em}[d] [nm]	τ_F[e] [ns]	τ_T[f] [μs]	Φ_Δ[g]	Φ_F[h]
An-BO	623	5.9	636	8.3	226	40	48
Ph-BO	613	5.4	643	11.3	215	12	73
BDP[i]	499	6.1	521	0.2	–[k]	–[k]	5
BDP-Me[j]	503	8.2	515	3.9	0.02	–[k]	71

[a] In acetonitrile (1.0×10^{-5} M). [b] UV/vis absorption maximum. [c] Molar absorption coefficient, ε: 10^4 M^{-1} cm^{-1}. [d] Fluorescence emission maximum. [e] Fluorescence lifetime. [f] Intrinsic triplet lifetime. [g] Singlet oxygen quantum yield (λ_{ex} = 630 nm, methylene blue used as standard compound, Φ_Δ = 57% in dichloromethane). [h] Absolute fluorescence quantum yield, determined with optical integrating sphere. [i] Parameters for **BDP** are taken from the literature.[82] [j] Parameters of **BDP-Me** are from the literature.[31] [k] Not observed.

Table 2 Singlet oxygen quantum yields (Φ_Δ) of **BO** derivatives in different solvents[a]

Compounds	HEX[b]	TOL[c]	THF[d]	DCM[e]	ACN[f]	MeOH[g]
An-BO	12	17	15	28	40	12
Ph-BO	5	7	6	10	12	5

[a] In percentage, λ_{ex} = 630 nm, methylene blue was used as standard, Φ_Δ = 57% in dichloromethane. [b] *n*-Hexane, $E_T(30)$ = 30.9 kcal mol^{-1}. [c] Toluene, $E_T(30)$ = 33.9 kcal mol^{-1}. [d] Tetrahydrofuran, $E_T(30)$ = 37.4 kcal mol^{-1}. [e] Dichloromethane, $E_T(30)$ = 41.1 kcal mol^{-1}. [f] Acetonitrile, $E_T(30)$ = 46.0 kcal mol^{-1}. [g] Methanol, $E_T(30)$ = 55.5 kcal mol^{-1}.

normalized absorption and fluorescence spectra, is 1.96 eV and 1.99 eV for **An-BO** and **Ph-BO**, respectively.

The fluorescence lifetimes of **An-BO** and **Ph-BO** were measured by time-correlated, single photon counting (TCSPC), using picosecond pulsed laser excitation (Fig. S13†). Both compounds gave mono-exponential decay curves, with lifetimes of 8.3 ns and 11.3 ns in ACN, respectively, for **An-BO** and **Ph-BO**. These lifetimes were found to be independent of solvent polarity. It is interesting to note that the measured lifetimes are considerably longer than those associated with conventional Bodipy emitters ($\tau_F \approx 4.0$ ns),[31,85,86] and of a recently reported Bodipy with twisted structure ($\tau_F \approx 3$ ns),[53,55,58] The radiative rate constants for **An-BO** and **Ph-BO** are lowered to *ca.* 6×10^7 s^{-1}, which is roughly half of that reported for conventional Bodipy-based chromophores. The photophysical properties of the target compounds are summarized in Table 1.

As a preliminary evaluation of the ISC efficiency of these compounds, the quantum yields for formation of singlet molecular oxygen (Φ_Δ) were measured (Table 2). For **Ph-BO**, $\Phi_\Delta \leq 12\%$ and dependent on solvent polarity; the highest yield was observed in ACN, with a much lower yield in HEX. The poor sensitization behaviour contrasts with that of the helicenes.[27,60,66] and with that of the twisted Bodipy, which shows Φ_Δ up to 55%.[53,55,57,58] Interestingly, an improved photosensitizing capability was observed for **An-BO**, where $\Phi_\Delta = 40\%$ in ACN and Φ_Δ = 12% in HEX (Table 2). Based on the absorption and fluorescence data, we propose that the weak dependence of the Φ_Δ values on the solvent polarity does not support the SOCT-ISC mechanism, as also demonstrated by femtosecond transient absorption spectroscopy (fs-TA, see later). However, the polarity of the solvent might affect the S_1/T_n energy matching, thereby influencing the yield of ISC, as found previously for anthracene (**An**).[87]

Electrochemical properties of the compounds

The redox potentials of the compounds were studied by cyclic voltammetry (Fig. 4a). For **Ph-BO**, an irreversible oxidation wave was observed at +0.67 V (*vs.* Fc/Fc^+) together with a reversible reduction wave at −1.35 V (*vs.* Fc/Fc^+) and an irreversible reduction wave at −2.17 V (*vs.* Fc/Fc^+). This behaviour is closely comparable with the previously reported results for the iodinated analogue of **Ph-BO**.[64]

Redox potentials were also determined for **An-BO**. At +1.12 eV there is a reversible oxidation wave, attributed to one-electron oxidation of the anthryl moiety,[88] compared to the known oxidation potential of anthracene (+0.9 V *vs.* Fc/Fc^+).[88,89] Making use of the Weller equation (eqn (S1)–(S3)†),[90–92] the Gibbs free energy change (ΔG_{CS}) accompanying intramolecular

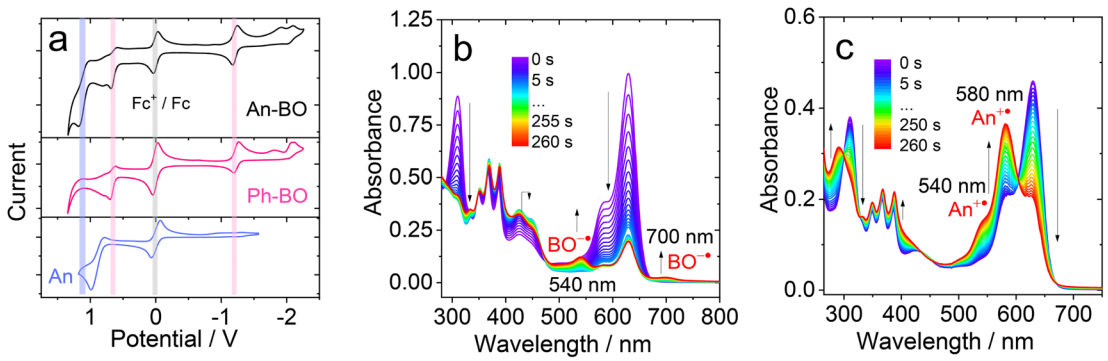

Fig. 4 Cyclic voltammograms determined for **BO** derivatives in deaerated ACN containing 0.10 M $Bu_4N[PF_6]$ as supporting electrolyte and with $Ag/AgNO_3$ as reference electrode. Scan rate: 100 mV s^{-1}. Ferrocene (Fc) was used as internal reference (set as 0 V in the cyclic voltammograms), $c = 1.0 \times 10^{-3}$ M. The absorption changes of **An-BO** upon (b) reduction with a potential of −1.40 V applied and (c) oxidation with a potential of +0.62 V applied on the working electrode. The spectra were recorded *in situ* with a spectroelectrochemical cuvette (1 mm optical path). $c = 1.0 \times 10^{-4}$ M in deaerated DCM. 20 °C.

Table 3 Redox potentials and driving forces of charge separation (ΔG_{CS}) and the projected energy of a charge-transfer state (CTS) for **BO** derivatives in different solvents[a]

	E_{RED}/V	E_{OX}/V	ΔG_{CS} (eV)/E_{CT} (eV) HEX	TOL	DCM	ACN
An	–[c]	+0.90	—[d]	—[d]	—[d]	—[d]
Ph-BO	−1.35/−2.17	+0.67	—[d]	—[d]	—[d]	—[d]
An-BO[b]	−1.39/−2.17	+0.67/+1.12	1.22/3.17	1.06/3.01	0.61/2.56	0.49/2.44

[a] Cyclic voltammetry in N_2-saturated ACN containing 0.1 M $Bu_4N[PF_6]$ as supporting electrolyte. Redox potentials of the compounds were determined with ferrocene (Fc) as internal standard (0 V). Counter electrode is Pt electrode and working electrode is glassy carbon electrode, with $Ag/AgNO_3$ couple as the reference electrode. [b] E_{00} = 1.96 eV. E_{00} is the energy level of singlet excited state localized on **BO** moiety (^{1}**BO***) approximated as the crossing point of normalized absorption and fluorescence spectra. [c] Not observed. [d] Not applicable.

electron transfer for **An-BO** (with E_{00} = 1.96 eV) was calculated (for details please refer to the ESI†). The main finding is a positive ΔG_{CS} in all solvents, a result in full agreement with the solvent-independent fluorescence properties found for **An-BO** (Fig. 3 and Table 3). Finally, spectroelectrochemistry was used to record absorption spectra for the **BO** radical anion ($BO^{-\bullet}$), with peaks at 540 nm and 700 nm, and the anthracene radical cation ($An^{+\bullet}$) with peaks at 540 nm and 580 nm (Fig. 4b and c). This latter information, used in conjunction with ultrafast transient absorption spectral measurements, helps to rule out the occurrence of light-induced charge separation.

Femtosecond transient absorption spectra: photoexcited state dynamics

The excited state dynamics of the target compounds were measured using femtosecond transient absorption (fs-TA) spectroscopy with a small series of solvents (HEX, DCM and ACN). For **An-BO**, excitation was made at both 360 nm, where the anthryl unit is an important absorber, and at 610 nm, where **BO** is the sole absorber. The fs-TA spectra of anthracene (**An**) in HEX were also recorded (Fig. 5a). The corresponding spectra are characterized by a strong excited state absorption (ESA) band centred at 420 nm and a weaker band centred at about 600 nm. Evolution associated difference spectra (EADS) were obtained by global analysis of the fs-TA data with a sequential model (Fig. 5b). The signal evolution on the picosecond timescale shows small changes in the spectral shape due to vibrational relaxation of the singlet excited state of **An**, indicating that both transient species (A and B) belong to singlet excited states and that vibrational relaxation occurs within 7 ps. The longer-living transient (species C) shows an ESA band centred at 420 nm and can be attributed to the $T_1 \rightarrow T_n$ transition. ISC occurs with a time constant of 2.5 ns, in good agreement with previous reports (τ_{ISC} = 2.3 ns).[88,89,93–95]

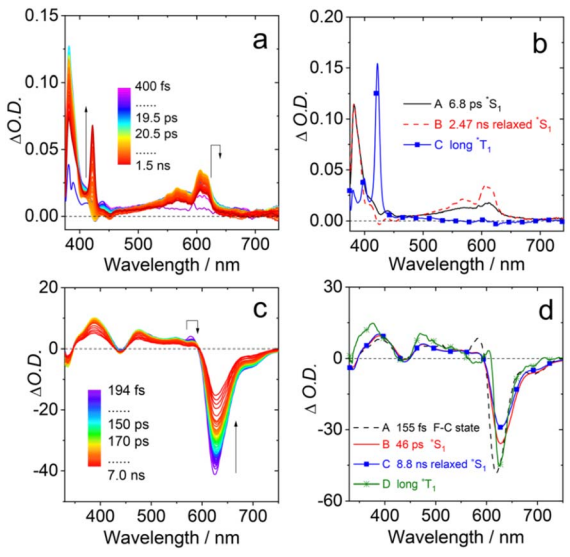

Fig. 5 Femtosecond transient absorption spectra of (a) **An** excited at 360 nm, (c) **Ph-BO** excited at 610 nm in ACN, and (b) EADS of **An**, (d) SADS of **Ph-BO** obtained with global analysis of the spectra reported in panels (a) and (c), respectively. $c = 1 \times 10^{-5}$ M.

Fig. 5c presents the fs-TA spectra of **Ph-BO** recorded in ACN following excitation at 610 nm. The transient spectra present an intense negative band centred at 630 nm, interpreted as the convolution between ground state bleaching (GSB) of the **BO** chromophore and stimulated emission (SE), with a weaker transient absorption band in the 380–600 nm range. The SE contributes mainly to the low-energy tail of the negative signal, extending beyond 740 nm. The transient bleaching gradually recovers over the timescale of the measurement, while the positive absorption band does not change significantly over time. Global analysis of the kinetic traces was applied to extract relevant time constants associated with evolution of the system (species associated difference spectra, SADS), using a target-model decay scheme comprising four species (Fig. 5d); the S_1 state of **Ph-BO** produces the triplet state with a low probability and relaxes to the ground state by radiative and non-radiative transitions.

The first component (black dashed curve) is assigned to a singlet excited state localized on the *N*,*N*,*O*,*O*-boron-chelated Bodipy. It is expected that excitation at 610 nm will populate the S_1 state with excess vibrational energy. The first ultrafast process, close to the detection limit of the instrument (155 fs) is assigned to a fast electronic relaxation bringing the system out of the initially populated Franck Condon state. Within 50 ps, the system evolves towards the third component, which retains similar spectral characteristics and is therefore ascribed to the S_1 state. Over this time interval, there is a small increase in the bleaching signal, that might be related to a red shift of the

emission band, together with a slight increase of ESA between 550 and 600 nm. These spectral perturbations can be assigned to relaxation of the excited state. Evolution to the final species occurs within *ca.* 9 ns, but the residual transient species is much longer lived than the maximum time window of the instrument. The profile of this residual signal is consistent with that of the triplet state observed in nanosecond transient absorption spectra (see below). This result indicates that the time constant for the decay of S_1 state is 8.8 ns, which is roughly in agreement with the long fluorescence lifetime of **Ph-BO** (11.3 ns, Table 1). **Ph-BO** has been studied also in HEX (Fig. S14†). The recorded transient spectra and the excited state evolution are similar to those observed in ACN, shown by the comparison between the kinetic traces recorded at the maximum of the GSB signal in ACN and HEX (Fig. S16†).

The fs-TA spectra recorded for **An-BO** in different solvents are comparable to those recorded for **Ph-BO**, thereby suggesting that formation of an intramolecular charge-transfer state is unimportant for this dyad (Fig. 6 and S15†). The spectral changes, however, do not rule out fast electronic energy transfer from anthracene to **BO** following excitation at 360 nm. Indeed, the component A with a lifetime close to the instrument detection limit, presents no SE signal, indicating that the higher singlet excited state is located on the anthryl unit (Fig. 6b). Subsequent spectra show a negative signal, with a minimum at 630 nm, attributable to a combination of GSB and SE of the **BO** unit. In addition, there is a weak absorption band extending from 380 to 600 nm. Target analysis performed in both HEX and ACN shows that spectral evolution occurs on different timescales compared to **Ph-BO**. The two components B and C have similar spectral character and are also similar to the singlet excited state signal of **Ph-BO** (Fig. 5d), so that, they can be assigned to the S_1 state and vibrationally relaxed S_1 state, respectively. The relaxation times, possibly including a contribution from intramolecular electronic energy transfer, are 24 ps and 31 ps, respectively in HEX and ACN. The residual species D shows ESA peaks at *ca.* 460 nm and 660 nm, and GSB peaks at 550 nm–650 nm (olive line in Fig. 6b); this spectral pattern can be attributed to the triplet-excited state of **An-BO** (see below). From the kinetics study, the time constants for the decay of S_1 of **An-BO** in HEX and ACN are 7.7 ns and 8.0 ns, respectively. When **An-BO** is excited at longer wavelength (610 nm, Fig. 6c and d), the first three components observed have similar shape. The GSB of the first component (black dotted line, component A, Fig. 6d) is slightly narrower than that of other two components, and has a somewhat stronger absorption at 590 nm; we attribute A to the unrelaxed singlet state. Solvation and vibrational relaxation occur within 250 fs and 50 ps, then the triplet state is produced (olive line). The lifetime of S_1 state is 6.7 ns. Transient absorption spectra for **An-BO** have been recorded also in polar solvents (Fig. S17 and S18†). The evolution of the transient spectra and the associated kinetics show only a minimal dependence on the solvent polarity.

Assuming internal conversion to the ground state is insignificant, the time constant for ISC can be approximated by $\tau_{ISC} = \tau_{S_1}/(1 - \Phi_F)$. An estimate for τ_{S_1} is available from the fs-TA studies, leading to the time constant for ISC for **Ph-BO** in acetonitrile as being *ca.* 33 ns, and that for **An-BO** as *ca.* 13 ns. This indicates that the rate of ISC for **An-BO** is roughly twice that for **Ph-BO**, which helps to account for the higher Φ_Δ for the former. Importantly, the ISC time constant is significantly shorter than that for conventional Bodipy derivatives.

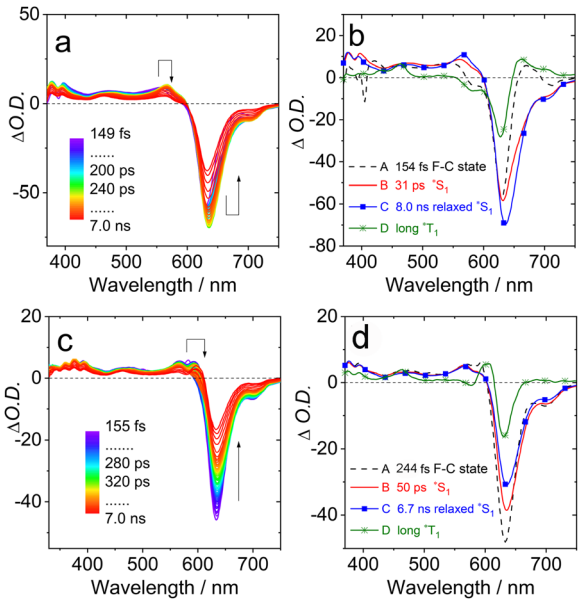

Fig. 6 Femtosecond transient absorption spectra for **An-BO** recorded in ACN, excited at (a) 360 nm and (c) 610 nm, the relative SADS obtained with global analysis are presented in panels (b) and (d), respectively, $c = 1.0 \times 10^{-5}$ M.

Nanosecond transient absorption (ns-TA) spectroscopy

The triplet excited states of the target compounds were studied by ns-TA spectroscopy in deoxygenated solution. The spectra recorded for **Ph-BO** show an ESA in the 350–500 nm range, overlapping with the ground state band at 410 nm (Fig. S19†). A significant GSB signal centred at 613 nm was also observed. The triplet state lifetime (τ_T) was determined as 192 μs. We developed a kinetic model to take into account triplet–triplet annihilation (TTA) effects, allowing the determination of the intrinsic triplet state lifetime[49,96,97] as being 215 μs. To the best of our knowledge, the ISC and triplet state of *N*,*N*,*O*,*O*-boron-chelated Bodipy were not studied previously. It might be noted that the red absorbing **Ph-BO** has a much longer triplet lifetime than the 2,6-diiodobisstyrylBodipy (τ_T = 1.8 μs) commonly portrayed as the prototypic red absorbing Bodipy species.[98]

For **An-BO**, a strong bleaching signal is observed at 622 nm, together with weaker absorption centred at 457 nm (Fig. 7). The intrinsic triplet lifetime was determined as 226 μs. This was shortened to 0.32 μs in aerated solution (Fig. S20†), confirming that the observed transient species is a triplet excited state localized on the Bodipy core. The ESA band of the *N*,*N*,*O*,*O*-boron coordinated Bodipy is drastically different from that observed for a bis-styrylBodipy, although the latter shows a similar absorption maximum to the *N*,*N*,*O*,*O*-boron

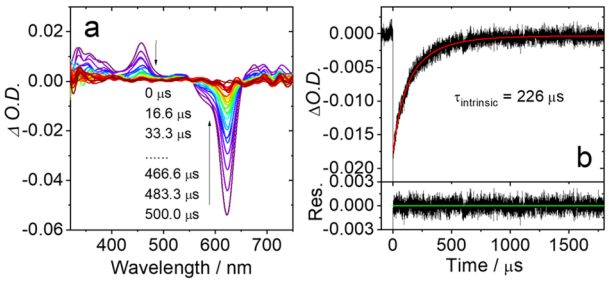

Fig. 7 (a) Nanosecond time-resolved transient absorption spectra recorded for **An-BO** upon pulsed laser excitation (λ_{ex} = 610 nm), (b) decay trace of **An-BO** at 605 nm in $c = 1.0 \times 10^{-6}$ M in deaerated acetonitrile, the intrinsic triplet state lifetime ($\tau_{intrinsic}$) was obtained by fitting the decay curves to the kinetic model taking into account triplet–triplet annihilation (TTA) (see the ESI† for details), the lifetime data in (b) were measured at 5×10^{-6} M, apparent lifetime is 209 μs. 25 °C.

coordinated Bodipy.[40,99,100] The intrinsic triplet lifetime of **An-BO** is much longer than that of Bodipy accessed with the heavy atom effect (153 μs),[101] or of the diiodobisstyrylBodipy (1.8 μs).[98] This is an important advantage of facilitating triplet population through the heavy atom-free protocal, *e.g.* by distorted framework approach, rather than the more conventional heavy-atom perturbation methodology.[17,102]

Neither of the target compounds is phosphorescent at room temperature or at 77 K. Estimates of the triplet state energies of **An-BO** and **Ph-BO** as being 1.35 eV and 1.38 eV, respectively, were obtained by TD-DFT computations (see ESI† for details). Also, an experimental determination of the triplet energy was made by intermolecular sensitization,[103] using *meso*-tetraphenylporphyrin (TPP, E_T = 1.44 eV) as triplet donor or perylenediimide (PBI, E_T = 1.20 eV) as triplet acceptor (Fig. S21 and S22†).[104] With this method, the triplet state energy of **An-BO** was determined to be *ca.* 1.24 eV. The T_1 state energies of these compounds are lower than that of the pristine Bodipy (*ca.* 1.6 eV),[105] but much higher than the bis-styrylBodipy (*ca.* 1.0 eV).[40,100] As such, promotion of the triplet-excited state through a twisted molecular structure[55,58] offers a promising route towards increasing absorption in the red region whilst maintaining a viable triplet state energy and long lifetime.[106]

Time-resolved electron paramagnetic resonance (TR-EPR) spectroscopy

Optical spectroscopy aids the identification of intermediate species and provides critical kinetic information but cannot give useful insight about the ISC electron spin selectivity or the zero field splitting (ZFS) of the triplet state. Moreover, knowledge of the extent of localization of the excitation energy in molecules with a large π-conjugated framework is a fundamental aspect of molecular photophysics and an important criterion for the successful design of new opto-electro materials.[107,108] The ZFS parameters *D* and *E* are important parameters of a chromophore, which may offer information about the spatial confinement of the triplet state wave function.[78,110–112] Specifically, the zero-field splitting parameter *D* is a measure of the delocalization of the unpaired electron of the triplet over the molecule, while *E* describes the nonaxial asymmetry (rhombicity) of the delocalization.[110,111]

The TR-EPR spectra of **Ph-BO** and **An-BO** recorded at 600 ns after the laser flash are presented in Fig. 8. The dependence of the TR-EPR and magnetophotoselection TR-EPR spectra of **Ph-BO** and **An-BO** on the delay time after photoexcitation are shown in the Fig. S25–S27†. The spectra are fully consistent with the involvement of a solitary triplet state. Furthermore, both the spectra and the consequent fitting parameters are comparable for the two compounds, clearly indicative of the localization of the triplet state on the **BO** fragment. The electron spin polarization (ESP) pattern for both compounds conforms to (*e*, *e*, *e*, *a*, *a*, *a*), this situation is reminiscent of that found for 2,6-diiodo-Bodipy,[49,97,113] and 2,6-diiodobisstyrylBodipy.[102] We previously observed the TR-EPR spectrum of the Bodipy triplet state, generated with the SOCT-ISC in compact anthryl-Bodipy orthogonal dyads, showing ESP phase pattern of (*e*, *e*, *e*, *a*, *a*, *a*), the SOCT-ISC mechanism can be excluded for **An-BO** based on the steady state fluorescence spectral study (Fig. 3b) and the fs-TA spectra (Fig. 6). Recently we found that the ESP of the triplet state TR-EPR spectrum of a twisted naphthalene-fused Bodipy is (*a*, *e*, *a*, *e*, *a*, *e*),[58] this indicates that the ESP of the triplet state of twisted Bodipy derivatives is highly dependent on the molecular structures.[56] This result shows the rich electron spin selectivity of the ISC of the twisted Bodipy derivatives.[62,114]

Simulation of the TR-EPR spectra gives ZFS *D* and *E* parameters for **Ph-BO** as −1470 MHz and 477 MHz, and almost the same for **An-BO** (Table 4). Similar *D* and *E* parameters indicate that the T_1 state of the molecules is confined on the **BO** chromophore. These parameters are different from those for 2,6-diiodoBodipy, for which the *D* and *E* values are −2940 MHz

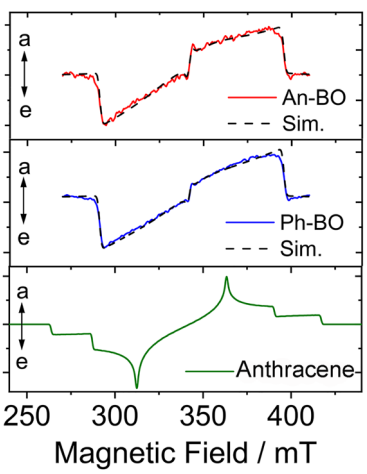

Fig. 8 Experimental TR-EPR spectra for **Ph-BO**, recorded at a delay time of 600 ns after laser excitation, the frozen samples ($c = 3.0 \times 10^{-4}$ M) were excited at 585 nm with a pulse energy of 1 mJ. For **An-BO**, the frozen samples ($c = 2.0 \times 10^{-4}$ M) were excited at 613 nm. The model TR-EPR spectrum of **An** calculated for D = 2150 MHz, E = 244 MHz, $P_z = 0.00$, $P_y = 0.56$, $P_x = 0.44$ (ref. 49 and 109) is also presented for comparison. Samples were dissolved in TOL/2-MeTHF (1/1, v/v), and the spectra were recorded at 80 K. Simulation parameters are presented in Table 4.

Table 4 ZFS parameters (D and E) and relative population rates $P_{x,y,z}$ of the zero-field spin states of the An-BO and Ph-BO. The data for a reference compound 2,6-diiodoBodipy are presented for comparison[a]

Compound	D^b (MHz)	E (MHz)	$P_x : P_y : P_z$
An-BO	−1470	467	0.00 : 0.00 : 1.00
Ph-BO	−1470	477	0.00 : 0.00 : 1.00
2,6-diiodoBodipy	−2940	655	0.00 : 0.15 : 1.00

[a] Obtained from simulation of the triplet-state TR-EPR spectra of the indicated molecules in a toluene/2-MeTHF glass (1/1, v/v) at 80 K. [b] The sign of the D parameter is negative for Bodipy.

and 655 MHz (Table 4), and the rhombicity (non-axiality) of the spatial distribution of the triplet state wave function $|E/D|$ is increased compared to the native Bodipy.[49,113] These results show that the triplet state wave functions are delocalized over the twisted molecular framework. Interestingly, the ZFS D and E parameters of **Ph-BO** and **An-BO** are similar to the recently reported naphthalene-fused Bodipy derivative, which also has a twisted molecular structure.[58] The population ratios of the sublevels of the T_1 state of **An-BO** remain similar to those of **Ph-BO** (Table 4), T_z sublevel of the T_1 state being overpopulated for both, which is supported by theoretical computations (see ESI† for more details).

DFT computation and the ISC mechanism

Density functional theory (DFT) calculations are often helpful in explaining photophysical behaviour. The molecular geometry of the ground state was optimized with DFT theory (Fig. 9). The dihedral angle between the dipyrrin ring and the anthryl moiety is 77° for **An-BO**, whereas that for **Ph-BO** is reduced to 47°. The twist angles between the planes defined by the two pyrrolic rings are 49° in both molecules, this being larger than the previously reported analogue (lacking the *meso*-substituent group, where the twist angle is *ca.* 10°).[65] The twist angle optimized by DFT is slightly different from that obtained by X-ray diffraction from a single crystal (Fig. 1). This is probably due to intermolecular interactions in the crystal. The similar torsion angles of the core chromophore in **Ph-BO** and **An-BO** unambiguously demonstrate that the disparate ISC efficiency of **An-BO** and **Ph-BO** is not caused by any different twisting of the chromophore, rather, it is due to the tuning of the excited states, by introducing the anthryl group in **An-BO**.

The electron spin density of the T_1 state was computed (Fig. 9c and d). For **An-BO**, the spin density is almost exclusively localized on the twisted Bodipy moiety, with negligible distribution on the anthryl unit. This seems consistent with the large dihedral angle between the anthryl moiety and the twisted Bodipy core (77°), which effectively decouples the two components. For **Ph-BO**, part of the spin density is distributed over the *meso*-phenyl ring, presumably because of the smaller dihedral angle. However, this disparate distribution of the triplet state electron spin density surface between the two triplets does not affect either the transient absorption or the TR-EPR spectra. For both compounds, the difference in electron density of the triplet excitation (corresponding to a HOMO → LUMO transition, Fig. S27†) is mainly localized on the twisted dipyrrin core.[68]

In order to further understand the difference in triplet state quantum yield of the compounds, we also studied the native oxo-Bodipy (**BO**), which has a hydrogen atom at the *meso* position. All electronic structure calculations were performed with the ORCA programs,[115,116] using DFT with the CAM-B3LYP functional and the def2-SVP atomic orbital basis set. The electronic ground state S_0 was optimized with restricted DFT, the T_1 state with unrestricted DFT, and all other excited states with TD-DFT. For each excited state the Hessian matrix was calculated and checked for positive definiteness. These optimized geometries and their Hessians are subsequently used in an excited state dynamic (ESD) calculation that yields the rate constant for ISC. Both Franck–Condon and Herzberg–Teller contributions were calculated for all three sublevels of each triplet state. We used a purpose-written program applying the formulae of Baiardi *et al.*[117] or of de Souza *et al.*,[118] which yield identical results.

With the CAM-B3LYP functional, the T_2 state is found below the S_1 state, hence the ISC rates for $S_1 \rightarrow T_2$ ISC were also calculated. The excitation energies calculated with the CAM-B3LYP functional for S_1 are substantially higher than the experimental values (see below), TD-DFT usually highly overestimates the low-lying excited states of Bodipy derivatives, hence it is possible that the true $S_1 \rightarrow T_2$ energy gap is small or

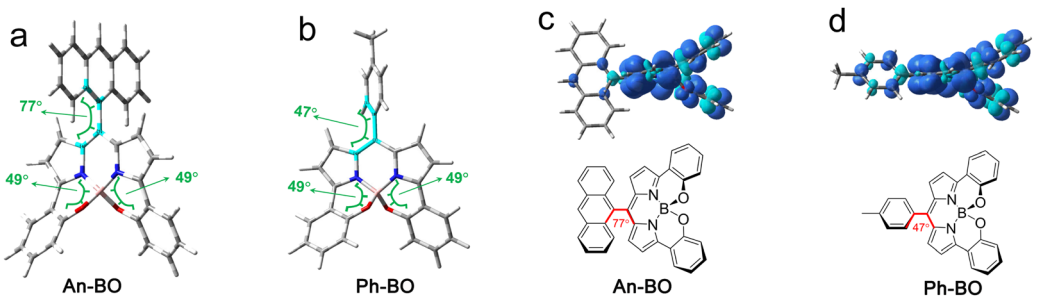

Fig. 9 Dihedral angles of selected atoms of (a) An-BO and (b) Ph-BO at the optimized ground state geometry, at CAM-B3LYP/6-31G (d) level with Gaussian 09; spin density surfaces of (c) An-BO and (d) Ph-BO at the optimized triplet state geometry; calculated at the CAM-B3LYP/6-31G(d) level with Gaussian 09W. Iso value of the spin density surfaces is 0.0015.

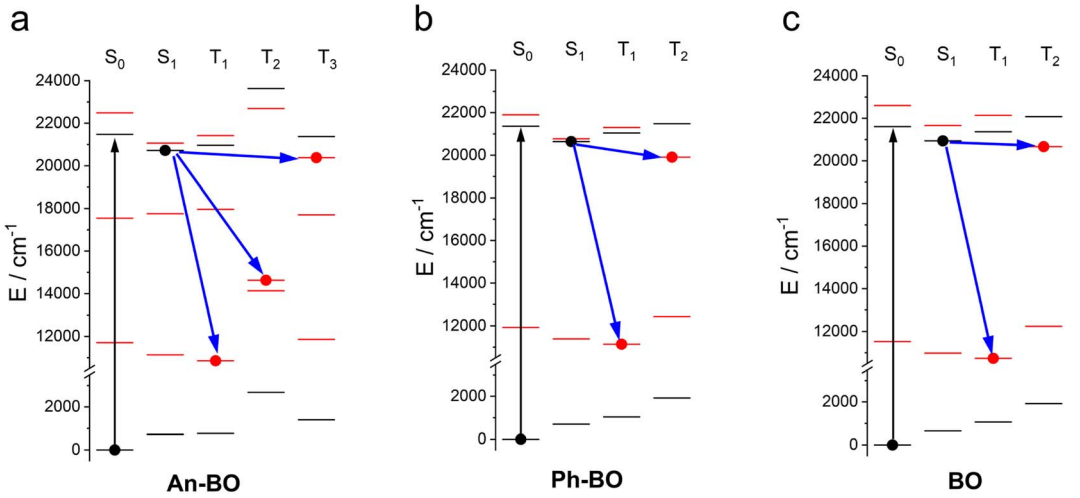

Scheme 2 Energy level diagrams for (a) An-BO, (b) Ph-BO and (c) BO at each of the optimized geometries. In each column, the optimized state is indicated by the full dot. Black lines indicate singlet states, red lines represent the triplet states, and blue arrows indicate the ISC transitions.

even negative. An exception is the T_2 state of **An-BO** which is a locally excited state on the anthryl unit and has no counterpart in the two other compounds. At each optimized geometry, the vertical excitation energies were calculated, resulting in the level diagrams shown in Scheme 2 (refer to Table S2† for specific values). For **Ph-BO**, both HOMO and LUMO are localized on the dipyrrin unit. The S_1 state is predominantly of HOMO → LUMO excitation (*i.e.*, a locally excited singlet state). Optimization of the S_1 state lowers its energy by *ca.* 1000 cm^{-1} with respect to the vertical excitation and shifts the S_0 state by about the same amount to higher energies (Table S2†), thus predicting a rather small Stokes shift. The geometrical change is small, and the dipole moment almost unchanged on excitation. For all three compounds, the T_1 state is found at about half of the energy of the S_1 state, but at almost the same geometry. A rather large exchange integral is indicated by the observation that T_1 also has a large contribution from the HOMO → LUMO excitation.

For **An-BO**, the T_2 state corresponds to excitation from the HOMO to the LUMO of the anthryl unit, *i.e.*, it is a locally excited state (^{3}**An***). Optimization of the geometry of this T_2 state leads to a strong stabilization accompanied by significant structural changes at the anthryl unit. At its minimum, the T_2 state is almost degenerate with the Bodipy-localized T_1 state. Since both the lower and the upper singly occupied orbitals in S_1 and T_2 are different, we expect small SOCMEs. Hence vibrationally induced SOC should be considered.[28,119] Indeed, we find that Herzberg–Teller coupling accounts for 100% of the ISC rates to the $M = +1/-1$ substates of the triplets, and for a substantial fraction of the $M = 0$ substate.

The program allows calculation of the ISC rate constant as a continuous function of the energy gap. Input data were the geometries and Hessians from the ORCA optimizations, as well as the SOCMEs and their derivatives with respect to all normal coordinates. Fig. 10a shows the resulting ISC rate constants (k_{ISC}) for the $S_1 \rightarrow T_1$ transition for each of the three compounds, the calculated energy gaps are indicated by a dot for each curve. We note that the rates of the $S_1 \rightarrow T_1$ transition are comparable for the three compounds, indicating that the anthryl substituent is not involved in this particular process. For energy gaps of *ca.* 10 000 cm^{-1}, these rates are smaller than 10^5 s^{-1} and hence cannot explain the observed triplet yields. This is most probably a consequence of the fact that S_1 and T_1 correspond to the same HOMO → LUMO excitation and therefore have rather small SOCME. However, for **An-BO**, the k_{ISC} of $S_1 \rightarrow T_2$ is greatly increased, which is consistent with the higher triplet yield. The $S_1 \rightarrow T_2$ transition in **An-BO** leads directly to the triplet state localized on the anthryl moiety.

Fig. 10b shows the corresponding data for ISC from the S_1 state to the second locally excited triplet on the **BO** unit, the relevant transitions are $S_1 \rightarrow T_2$ for **BO** and **Ph-BO**, and $S_1 \rightarrow T_3$ for **An-BO**. As in the case of the $S_1 \rightarrow T_2$ transitions, these curves are comparable, indicating that these triplet states are associated with the **BO** unit and have similar orbital excitation character. The substituents appear not to be involved. Since orbitals

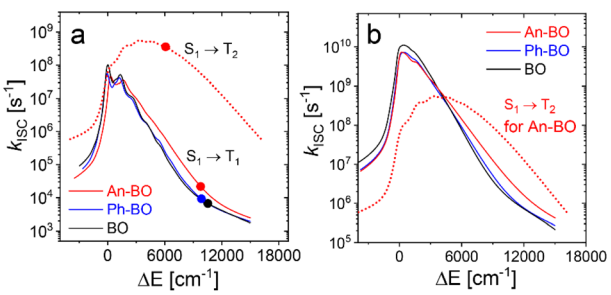

Fig. 10 Energy gap dependence of the ISC rate constants (Franck–Condon plus Herzberg–Teller terms). (a) Rate constants for the $S_1 \rightarrow T_1$ transitions of **An-BO** (red line), **Ph-BO** (blue line) and **BO** (black line), the red dotted line refers the $S_1 \rightarrow T_2$ transition of **An-BO**. The calculated energy gap is indicated by a dot in each curve. (b) Energy gap dependence of the ISC rate constant for $S_1 \rightarrow T_n$ transitions. The full lines are for the second local triplet of the **BO** unit, which is T_2 in **BO** and **Ph-BO**, but T_3 in **An-BO**. The dotted line is for T_2 of **An-BO** which is a local triplet on the anthryl unit.

other than those associated with S_1 are involved, the SOCMEs are increased, thereby enhancing the rate constants by two orders of magnitude compared to $S_1 \rightarrow T_1$. The rate constant for the $S_1 \rightarrow T_2$ transition for **An-BO** shows significantly different behaviour to that of the other compounds (dotted line in Fig. 10). The final state T_2 is a locally excited triplet of the anthryl unit which has no low-energy counterpart in the parent compound or the phenyl-derivative (*i.e.*, ISC corresponds to intramolecular energy transfer). The transition is accompanied by a strong geometrical relaxation within the anthryl unit, giving a broad profile to the energy gap dependence.

The second local triplet state on the **BO** unit is probably at higher energy than the S_1 state, *i.e.* the energy gap is negative. A gap in the range (1500–1000) cm^{-1} would still allow ISC to occur with a rate constant of *ca.* 10^8 s^{-1}. There is little experimental information on the true energy gap between S_1 and T_2 in these compounds. It is hence possible that the T_2 states of **BO** and **Ph-BO** in reality are higher than S_1. On the other hand, the strong relaxation of T_2 observed for **An-BO** suggests that the state is near T_1 and below S_1. Unsubstituted anthracene has a T_1 state energy of 1.8 eV.[104] This is below the experimental energy for the S_1 state of **Ph-BO** (*ca.* 2.0 eV). For an energy gap in the range 4000–6000 cm^{-1} the calculations anticipate ISC rate constants near 5×10^8 s^{-1}. These are in good agreement with a triplet yield in the range of 50%. It must then be concluded that the actual $S_1 \rightarrow T_2$ energy gap in **Ph-BO** is negative, *i.e.*, T_2 is above S_1. Thus, the increased rate of ISC for **An-BO** can be ascribed to transient population of the T_2 state localized on the anthryl unit.

This is an interesting example whereby the initial and the final states of ISC are confined on different chromophores, yet the matching of the S_1 and T_2 state energies (at the geometry of S_1) still induces efficient ISC. This result may present new understanding of singlet-to-triplet energy transfer, which is much less common than singlet–singlet or triplet–triplet energy transfer.[120,121] Our theoretical studies are able to correctly predict that the T_z sublevel of the T_1 states of the compounds are overpopulated, which is in agreement with the TR-EPR spectral observations (see ESI for more details, Fig. S30 and S31†). We found that the SOCME favours the transition to the T_x-substate, while the much larger vibrational contributions favour the transition to the T_z-state, which is in agreement with the TR-EPR spectral experimental results (Fig. 8 and Table 4). This principal is applicable to other twisted molecules, *i.e.* the ESP phase pattern of the T_1 state TREPR spectrum of a compound, should be directly related to the ISC rate constants of $S_1 \rightarrow T_x$, $S_1 \rightarrow T_y$ and $S_1 \rightarrow T_z$.

Because of the stated uncertainties about the S_1 state energy obtained by the TD-DFT calculation, we prefer to rely on the values obtained experimentally. The absence of detectable levels of phosphorescence, however, precludes any experimental T_1 state energy, and we must rely on the computed results. This leads to the simplified energy diagrams for **An-BO** and **Ph-BO** shown in Scheme 3. For **Ph-BO**, the T_2 state energy is higher than that of S_1, and there is a large energy gap between S_1 and T_1 states, making ISC inefficient. For **An-BO**, the T_2 state (*i.e.*, 1.81 eV), localized on the anthryl moiety, is lower in energy than the S_1 state (*i.e.*, 1.96 eV), thereby facilitating faster ISC through intermediary population of the anthryl triplet state. Notably, triplet population *via* this route involves two separate electronic energy transfer events rather than the conventional SOC mechanism.

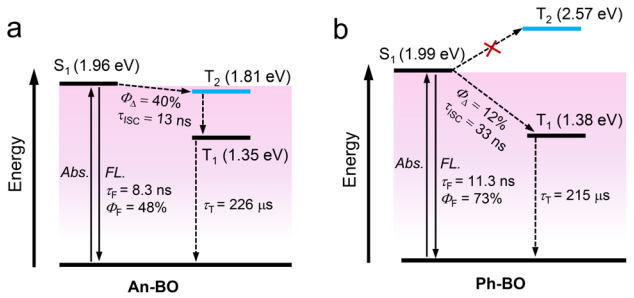

Scheme 3 Simplified Jablonski diagram illustrating the photophysical processes involved in (a) **An-BO** and (b) **Ph-BO** upon photoexcitation. Energy level of S_1 is taken as the intersection of absorption and luminescence spectra, and the triplet energy is from the TD-DFT calculation.

Conclusion

This study represents an attempt to identify ways to enhance intersystem crossing (ISC), leading to triplet formation, for heavy atom-free organic chromophores, which usually have slow ISC kinetics. The common rationale for promoting ISC in such materials relies on incorporating a heavy atom into the π-system, but this has several disadvantages. The main concept under investigation here relates to the notion that a severely twisted π-conjugation framework, such as that inherent to the family of *N*,*N*,*O*,*O*-boron-chelated Bodipy chromophores, serves to promote ISC without the undesired consequences of heavy atom substituents. Our results indicate that ISC is indeed enhanced through this treatment but this is not a major effect. Thus, **Ph-BO** shows only a modest singlet oxygen quantum yield ($\Phi_\Delta = 12\%$) and a time constant for ISC of *ca.* 33 ns. However, this strategy pushes the absorption bands into the red region, in marked contrast with the effects of halogenation, and this is highly beneficial. The limited performance with **Ph-BO**, which contrasts with the ISC behaviour of the helicenes, can be traced to a large $S_1 \rightarrow T_1$ energy gap, combined with weak $S_1 \rightarrow T_2$ coupling. Time-resolved electron paramagnetic resonance spectra of the triplet show an electron spin polarization phase pattern of (*e*, *e*, *e*, *a*, *a*, *a*). Zero field splitting *D* and *E* parameters of the triplet state of the twisted Bodipy chromophore indicate the triplet wave function is spread over the distorted π-conjugation framework. The main finding from these various studies is that the twisted π-conjugation does not necessarily promote ISC.

To overcome the large $S_1 \rightarrow T_1$ energy gap, the *meso*-phenyl ring has been replaced with an anthryl moiety which has a locally-excited triplet state of comparable energy to the S_1 state associated with the twisted Bodipy chromophore. For this dyad, **An-BO**, charge recombination-induced ISC is insignificant, as

demonstrated by steady-state optical spectra and fs-TA measurements. The triplet quantum yield is increased substantially and **An-BO** exhibits a much improved quantum yield for formation of singlet molecular oxygen ($\Phi_\Delta = 40\%$). The greater propensity towards triplet formation must arise from increased coupling between the S_1 and T_2 states. It is important to stress that these two excited states are localized on different chromophores and held in a near orthogonal geometry but still manage to promote ISC. Transient population of the anthryl-based triplet state is followed by triplet–triplet energy transfer to form the T_1 state localized on the Bodipy fragment. The latter process is spin-allowed and likely to be fast but the former step is relatively slow because of the molecular orientation and limited spectral overlap. Nonetheless, the process competes with fluorescence and internal conversion from S_1. The overall ISC rate for **An-BO** is faster (*ca.* 13 ns) than for **Ph-BO**. In this respect, it is important to note that these Bodipy derivatives based on twisted π-conjugation pathways show unusually long-lived S_1 states and this is a considerable benefit in terms of applications. Our results show that the twisted π-conjugation system cannot be relied upon to induce efficient ISC. An improved strategy is based on energy matching of S_1/T_n ($n > 1$) states. Moreover, since the anthryl triplet is far from optimal as an acceptor, there is considerable scope to design a new range of heavy atom-free triplet sensitizers along these lines.

Experimental section

General method

All chemicals used for synthesis were analytically pure and used as received. Solvents were dried and distilled prior to use. Samples of **Ph-BO** were prepared as before and we thank Dr J. G. Knight (Newcastle University) for providing a sample for preliminary spectroscopic investigations.[64,65] The UV/vis absorption spectra were recorded with a UV2550 spectrophotometer (Shimadzu Ltd, Japan). The fluorescence spectra were recorded with an FS5 spectrofluorometer (with photon counting detection method. Edinburgh Instruments, UK). The fluorescence lifetimes of compounds were measured with an OB920 luminescence lifetime spectrometer (Edinburgh Instruments, UK), an EPL picosecond pulsed laser was used for excitation, and time-correlated, single photon counting (TCSPC) was used for detection.

Nanosecond transient absorption spectroscopy

The nanosecond transient absorption spectra were acquired on a LP980 laser flash photolysis spectrometer (Edinburgh Instruments, UK). The signal was digitized with a Tektronix TDS 3012B oscilloscope. Samples were excited with a nanosecond pulsed laser (Surelite I-10, USA; the wavelength being tunable in the range of 210–2400 nm). Typical laser energy was 5 mJ per pulse. The samples were deaerated with N_2 for 15 min.

Femtosecond transient absorption spectroscopy

Femtosecond transient absorption spectra were measured by an ultrafast transient absorption spectrometer (Harpia-TA, Light Conversion). A Ti:sapphire laser amplifier (Astrella Coherent) with 40 fs pulse duration at 800 nm and 1 kHz repetition rate was used for these experiments. The white-light-continuum probe pulses were generated by a 2 mm CaF_2 nonlinear crystal, and spectrally tunable pump pulses were generated by an optical parametric amplifier (TOPAS-C, light conversion). A 1 mm pathlength quartz cuvette housed the solution. Changes in absorbance were monitored by focusing the transmitted probe light through the solution onto a broadband UV/vis detector. Data analysis was performed applying Singular Value Decomposition (SVD) and global analysis with target model, using the software GLOTARAN.[122]

TR-EPR spectroscopy

TR-EPR spectral measurements were carried out at 80 K. Samples were excited at 532–613 nm, 1 mJ pulse,10 ns, 100 Hz using the output of an optical parametric oscillator (LP603 SOLAR Laser Systems), pumped with the output of a Nd:YAG laser (LQ629 SOLAR Laser Systems). Samples were dissolved in toluene/2-methyltetrahydrofuran (1/1, v/v), with subsequent removal of dissolved air by freeze–pump–thaw cycles. The time-resolved continuous-wave EPR spectral measurements were performed on an EPR Elexsys E-580 spectrometer (Bruker) with a flexlinel resonator (ER 4118X-MD5-W1) at X-band at 80 K. Low temperature measurements were carried out in a CF935 cryostat (Oxford Instruments) cooled by liquid nitrogen. The TR-CW EPR spectra were obtained by the summation of the data in different time windows after the laser pulse. The EPR spectra were simulated using the Easy Spin package implemented in the MATLAB programming language.[123]

Theoretical computation

Geometries for the electronic ground state and for the lowest-excited triplet state were optimized with density functional theory (DFT) at the CAM-B3LYP/6-31G(d) level, using the Gaussian 09W program.[124] All structures were minima on the potential energy surface, since all eigenvalues of the Hessians were positive. The spin orbit coupling matrix elements (SOCME), and their derivatives along the normal coordinates, were calculated between S_1 and all triplet states with the ORCA program at the CAM-B3LYP/def2-SVP level. These data were subsequently used by a purpose-built program which calculates the ISC rates (both Franck–Condon and Herzberg Teller contributions) as a function of the diabatic energy gaps between S_1 and each final triplet state. This program applies the formulae of Baiardi *et al.*[117] or of de Souza *et al.*[118] originally developed for calculation of emission spectra, but which can be modified for ISC. Specifically, we replaced the three components of the transition dipole matrix elements by the SOCME for the three sublevels, also replacing their derivatives with respect to the normal coordinates. In these modified formulae, the energy gap can be regarded as a variable parameter, such that instead of a spectrum one gets the energy-gap dependence of the ISC rate constant. The SOCME and their derivatives are calculated with the ESD module of the ORCA program. These use the RI-SOMF(1X) option of ORCA, *i.e.*, the mean-field

operator (effective potentials), including one-electron terms. Coulomb terms are computed with the resolution of identity approximation, exchange terms use one-center exact integrals including the spin-other orbit interaction, and DFT local correlation terms are not included.

Data availability

All relevant data are presented in the main text and/or ESI.†

Author contributions

X. Z., A. A. S. and X. L. contributed equally to this work. J. Z. conceived the research, directed the analysis of the results; X. Z. synthesized the compounds, measured and analysed steady-state optical spectra, electrochemistry, transient absorption spectra and other photophysical processes; A. A. S. and V. K. V. measured and simulated TR-EPR spectra; X. L., Y. W, M. T. and M. D. D. measured and analysed femtosecond transient absorption spectroscopy; A. H. provided guidance on the analysis of parts of the photophysical studies and revised parts of the manuscript; B. D. performed the theoretical computational analysis. All authors provided comments on preparation and modification of the manuscript.

Conflicts of interest

There are no conflicts to declare.

Acknowledgements

J. Z. thanks the NSFC (U2001222), the Research and Innovation Team Project of Dalian University of Technology (DUT2022TB10), the Fundamental Research Funds for the Central Universities (DUT22LAB610) and the State Key Laboratory of Fine Chemicals for financial support. M. D. D acknowledges support from the European Union's Horizon 2020 research and innovation program under grant agreement 871124 Laserlab-Europe. A. A. S. and V. K. V. acknowledge financial support from the government assignment for the Federal Research Center (Kazan Scientific Center of Russian Academy of Sciences). B. D. thanks the Dalian University of Technology for support through a HaiTian Professorship. X. Z. thanks the support of "the Fundamental Research Funds for the Central Universities".

Notes and references

1 A. Kamkaew, S. H. Lim, H. B. Lee, L. V. Kiew, L. Y. Chung and K. Burgess, *Chem. Soc. Rev.*, 2013, **42**, 77–88.
2 J. Zhao, W. Wu, J. Sun and S. Guo, *Chem. Soc. Rev.*, 2013, **42**, 5323–5351.
3 J. Zhao, K. Xu, W. Yang, Z. Wang and F. Zhong, *Chem. Soc. Rev.*, 2015, **44**, 8904–8939.
4 J. M. R. Narayanam and C. R. J. Stephenson, *Chem. Soc. Rev.*, 2011, **40**, 102–113.
5 L. Shi and W. Xia, *Chem. Soc. Rev.*, 2012, **41**, 7687–7697.
6 D. Ravelli, M. Fagnoni and A. Albini, *Chem. Soc. Rev.*, 2013, **42**, 97–113.
7 S. Fukuzumi and K. Ohkubo, *Chem. Sci.*, 2013, **4**, 561–574.
8 J. I. Goldsmith, W. R. Hudson, M. S. Lowry, T. H. Anderson and S. Bernhard, *J. Am. Chem. Soc.*, 2005, **127**, 7502–7510.
9 G.-G. Luo, H. Lu, X.-L. Zhang, J.-C. Dai, J.-H. Wu and J.-J. Wu, *Phys. Chem. Chem. Phys.*, 2015, **17**, 9716–9729.
10 G.-G. Luo, K. Fang, J.-H. Wu and J. Mo, *Chem. Commun.*, 2015, **51**, 12361–12364.
11 P. Wang, S. Guo, H.-J. Wang, K.-K. Chen, N. Zhang, Z.-M. Zhang and T.-B. Lu, *Nat. Commun.*, 2019, **10**, 3155.
12 S. Guo, K.-K. Chen, R. Dong, Z.-M. Zhang, J. Zhao and T.-B. Lu, *ACS Catal.*, 2018, **8**, 8659–8670.
13 S. Sato, T. Morikawa, T. Kajino and O. Ishitani, *Angew. Chem., Int. Ed.*, 2013, **52**, 988–992.
14 Y. Tamaki, K. Koike, T. Morimoto, Y. Yamazaki and O. Ishitani, *Inorg. Chem.*, 2013, **52**, 11902–11909.
15 P. Wang, R. Dong, S. Guo, J. Zhao, Z.-M. Zhang and T.-B. Lu, *Natl. Sci. Rev.*, 2020, **7**, 1459–1467.
16 X. Li, S. Kolemen, J. Yoon and E. U. Akkaya, *Adv. Funct. Mater.*, 2017, **27**, 1604053.
17 V.-N. Nguyen, Y. Yan, J. Zhao and J. Yoon, *Acc. Chem. Res.*, 2021, **54**, 207–220.
18 J. Tian, J. Zhou, Z. Shen, L. Ding, J.-S. Yu and H. Ju, *Chem. Sci.*, 2015, **6**, 5969–5977.
19 Q. Tang, W. Xiao, J. Li, D. Chen, Y. Zhang, J. Shao and X. Dong, *J. Mater. Chem. B*, 2018, **6**, 2778–2784.
20 M.-R. Ke, S.-L. Yeung, D. K. P. Ng, W.-P. Fong and P.-C. Lo, *J. Med. Chem.*, 2013, **56**, 8475–8483.
21 D. Chen, Z. Zhong, Q. Ma, J. Shao, W. Huang and X. Dong, *ACS Appl. Mater. Interfaces*, 2020, **12**, 26914–26925.
22 J. Zhao, S. Ji and H. Guo, *RSC Adv.*, 2011, **1**, 937–950.
23 T. N. Singh-Rachford and F. N. Castellano, *Coord. Chem. Rev.*, 2010, **254**, 2560–2573.
24 C. Ye, L. Zhou, X. Wang and Z. Liang, *Phys. Chem. Chem. Phys.*, 2016, **18**, 10818–10835.
25 N. Yanai and N. Kimizuka, *Acc. Chem. Res.*, 2017, **50**, 2487–2495.
26 N. J. Turro, V. Ramamurthy and J. C. Scaiano, *Principles of Molecular Photochemistry: An Introduction*, University Science Books, Sausalito, CA, 2009.
27 K. Schmidt, S. Brovelli, V. Coropceanu, D. Beljonne, J. Cornil, C. Bazzini, T. Caronna, R. Tubino, F. Meinardi, Z. Shuai and J.-L. Brédas, *J. Phys. Chem. A*, 2007, **111**, 10490–10499.
28 Z. Mahmood, A. A. Sukhanov, N. Rehmat, M. Hu, A. Elmali, Y. Xiao, J. Zhao, A. Karatay, B. Dick and V. K. Voronkova, *J. Phys. Chem. B*, 2021, **125**, 9317–9332.
29 T. Yogo, Y. Urano, Y. Ishitsuka, F. Maniwa and T. Nagano, *J. Am. Chem. Soc.*, 2005, **127**, 12162–12163.
30 M. Nakashima, K. Iizuka, M. Karasawa, K. Ishii and Y. Kubo, *J. Mater. Chem. C*, 2018, **6**, 6208–6215.
31 W. Wu, H. Guo, W. Wu, S. Ji and J. Zhao, *J. Org. Chem.*, 2011, **76**, 7056–7064.
32 A. Gorman, J. Killoran, C. O'Shea, T. Kenna, W. M. Gallagher and D. F. O'Shea, *J. Am. Chem. Soc.*, 2004, **126**, 10619–10631.

33 N. Adarsh, R. R. Avirah and D. Ramaiah, *Org. Lett.*, 2010, **12**, 5720–5723.
34 V.-N. Nguyen, S. Qi, S. Kim, N. Kwon, G. Kim, Y. Yim, S. Park and J. Yoon, *J. Am. Chem. Soc.*, 2019, **141**, 16243–16248.
35 A. J. Tilley, R. D. Pensack, T. S. Lee, B. Djukic, G. D. Scholes and D. S. Seferos, *J. Phys. Chem. C*, 2014, **118**, 9996–10004.
36 M. Bröring, R. Krüger, S. Link, C. Kleeberg, S. Köhler, X. Xie, B. Ventura and L. Flamigni, *Chem. – Eur. J.*, 2008, **14**, 2976–2983.
37 B. Ventura, G. Marconi, M. Bröring, R. Krüger and L. Flamigni, *New J. Chem.*, 2009, **33**, 428–438.
38 Z. Zhu, X. Zhang, X. Guo, Q. Wu, Z. Li, C. Yu, E. Hao, L. Jiao and J. Zhao, *Chem. Sci.*, 2021, **12**, 14944–14951.
39 W. Wu, J. Zhao, J. Sun and S. Guo, *J. Org. Chem.*, 2012, **77**, 5305–5312.
40 L. Huang, X. Yu, W. Wu and J. Zhao, *Org. Lett.*, 2012, **14**, 2594–2597.
41 Y. Wei, M. Zhou, Q. Zhou, X. Zhou, S. Liu, S. Zhang and B. Zhang, *Phys. Chem. Chem. Phys.*, 2017, **19**, 22049–22060.
42 R. Ziessel, B. D. Allen, D. B. Rewinska and A. Harriman, *Chem. – Eur. J.*, 2009, **15**, 7382–7393.
43 J.-Y. Liu, M. E. El-Khouly, S. Fukuzumi and D. K. P. Ng, *Chem. – Asian J.*, 2011, **6**, 174–179.
44 C. B. KC, G. N. Lim, V. N. Nesterov, P. A. Karr and F. D'Souza, *Chem. – Eur. J.*, 2014, **20**, 17100–17112.
45 Z. Wang, J. Zhao, A. Barbon, A. Toffoletti, Y. Liu, Y. An, L. Xu, A. Karatay, H. G. Yaglioglu, E. A. Yildiz and M. Hayvali, *J. Am. Chem. Soc.*, 2017, **139**, 7831–7842.
46 Z. Wang, Y. Gao, M. Hussain, S. Kundu, V. Rane, M. Hayvali, E. A. Yildiz, J. Zhao, H. G. Yaglioglu, R. Das, L. Luo and J. Li, *Chem. – Eur. J.*, 2018, **24**, 18663–18675.
47 X. Zhang, A. A. Sukhanov, E. A. Yildiz, Y. E. Kandrashkin, J. Zhao, H. G. Yaglioglu and V. K. Voronkova, *Chemphyschem*, 2021, **22**, 55–68.
48 M. A. Filatov, S. Karuthedath, P. M. Polestshuk, H. Savoie, K. J. Flanagan, C. Sy, E. Sitte, M. Telitchko, F. Laquai, R. W. Boyle and M. O. Senge, *J. Am. Chem. Soc.*, 2017, **139**, 6282–6285.
49 Z. Wang, A. A. Sukhanov, A. Toffoletti, F. Sadiq, J. Zhao, A. Barbon, V. K. Voronkova and B. Dick, *J. Phys. Chem. C*, 2019, **123**, 265–274.
50 X. Zhang, Z. Wang, Y. Hou, Y. Yan, J. Zhao and B. Dick, *J. Mater. Chem. C*, 2021, **9**, 11944–11973.
51 E. Bassan, A. Gualandi, P. G. Cozzi and P. Ceroni, *Chem. Sci.*, 2021, **12**, 6607–6628.
52 Y. Wu, Y. Zhen, Y. Ma, R. Zheng, Z. Wang and H. Fu, *J. Phys. Chem. Lett.*, 2010, **1**, 2499–2502.
53 H. Ito, H. Sakai, Y. Suzuki, J. Kawamata and T. Hasobe, *Chem. – Eur. J.*, 2020, **26**, 316–325.
54 K. Nagarajan, A. R. Mallia, K. Muraleedharan and M. Hariharan, *Chem. Sci.*, 2017, **8**, 1776–1782.
55 Y. Dong, B. Dick and J. Zhao, *Org. Lett.*, 2020, **22**, 5535–5539.
56 Y. Dong, P. Kumar, P. Maity, I. Kurganskii, S. Li, A. Elmali, J. Zhao, D. Escudero, H. Wu, A. Karatay, O. F. Mohammed and M. Fedin, *Phys. Chem. Chem. Phys.*, 2021, **23**, 8641–8652.
57 Y. Yan, A. A. Sukhanov, M. H. E. Bousquet, Q. Guan, J. Zhao, V. K. Voronkova, D. Escudero, A. Barbon, Y. Xing, G. G. Gurzadyan and D. Jacquemin, *J. Phys. Chem. B*, 2021, **125**, 6280–6295.
58 Z. Wang, L. Huang, Y. Yan, A. M. El-Zohry, A. Toffoletti, J. Zhao, A. Barbon, B. Dick, O. F. Mohammed and G. Han, *Angew. Chem., Int. Ed.*, 2020, **59**, 16114–16121.
59 L. Shi, Z. Liu, G. Dong, L. Duan, Y. Qiu, J. Jia, W. Guo, D. Zhao, D. Cui and X. Tao, *Chem. – Eur. J.*, 2012, **18**, 8092–8099.
60 T. Biet, K. Martin, J. Hankache, N. Hellou, A. Hauser, T. Bürgi, N. Vanthuyne, T. Aharon, M. Caricato, J. Crassous and N. Avarvari, *Chem. – Eur. J.*, 2017, **23**, 437–446.
61 Y. Dong, M. Taddei, S. Doria, L. Bussotti, J. Zhao, G. Mazzone and M. Di Donato, *J. Phys. Chem. B*, 2021, **125**, 4779–4793.
62 Z. Wang, X. Zhang and J. Zhao, *J. Phys. Chem. C*, 2021, **125**, 19097–19109.
63 S. V. K. Isukapalli and S. R. Vennapusa, *J. Phys. Chem. A*, 2022, **126**, 7606–7612.
64 H. Kim, A. Burghart, M. B. Welch, J. Reibenspies and K. Burgess, *Chem. Commun.*, 1999, 1889–1890.
65 R. B. Alnoman, S. Rihn, D. C. O'Connor, F. A. Black, B. Costello, P. G. Waddell, W. Clegg, R. D. Peacock, W. Herrebout, J. G. Knight and M. J. Hall, *Chem. – Eur. J.*, 2016, **22**, 93–96.
66 M. Sapir and E. V. Donckt, *Chem. Phys. Lett.*, 1975, **36**, 108–110.
67 A. Loudet, R. Bandichhor, K. Burgess, A. Palma, S. O. McDonnell, M. J. Hall and D. F. O'Shea, *Org. Lett.*, 2008, **10**, 4771–4774.
68 S. Yamazawa, M. Nakashima, Y. Suda, R. Nishiyabu and Y. Kubo, *J. Org. Chem.*, 2016, **81**, 1310–1315.
69 S. Y. Leblebici, L. Catane, D. E. Barclay, T. Olson, T. L. Chen and B. Ma, *ACS Appl. Mater. Interfaces*, 2011, **3**, 4469–4474.
70 S. Y. Leblebici, T. L. Chen, P. Olalde-Velasco, W. Yang and B. Ma, *ACS Appl. Mater. Interfaces*, 2013, **5**, 10105–10110.
71 Y. Kubo, T. Shimada, K. Maeda and Y. Hashimoto, *New J. Chem.*, 2020, **44**, 29–37.
72 M. Saikawa, T. Nakamura, J. Uchida, M. Yamamura and T. Nabeshima, *Chem. Commun.*, 2016, **52**, 10727–10730.
73 R. D. Rieth, N. P. Mankad, E. Calimano and J. P. Sadighi, *Org. Lett.*, 2004, **6**, 3981–3983.
74 L. Copey, L. Jean-Gérard, E. Framery, G. Pilet and B. Andrioletti, *Eur. J. Org. Chem.*, 2014, **2014**, 4759–4766.
75 X.-Y. Zhu, H. Wu, X.-F. Guo and H. Wang, *Dyes Pigm.*, 2019, **165**, 400–407.
76 M. A. Filatov, *Org. Biomol. Chem.*, 2020, **18**, 10–27.
77 D. J. Gibbons, A. Farawar, P. Mazzella, S. Leroy-Lhez and R. M. Williams, *Photochem. Photobiol. Sci.*, 2020, **19**, 136–158.
78 Y. Hou, X. Zhang, K. Chen, D. Liu, Z. Wang, Q. Liu, J. Zhao and A. Barbon, *J. Mater. Chem. C*, 2019, **7**, 12048–12074.
79 W. Yang, J. Zhao, C. Sonn, D. Escudero, A. Karatay, H. G. Yaglioglu, B. Küçüköz, M. Hayvali, C. Li and D. Jacquemin, *J. Phys. Chem. C*, 2016, **120**, 10162–10175.

80 Z. Yu, Y. Wu, Q. Peng, C. Sun, J. Chen, J. Yao and H. Fu, *Chem. – Eur. J.*, 2016, **22**, 4717–4722.
81 Y. Tomimori, T. Okujima, T. Yano, S. Mori, N. Ono, H. Yamada and H. Uno, *Tetrahedron*, 2011, **67**, 3187–3193.
82 K. Chen, M. Taddei, L. Bussotti, P. Foggi, J. Zhao and M. Di Donato, *ChemPhotoChem*, 2020, **4**, 487–501.
83 S. Sasaki, K. Hattori, K. Igawa and G.-i. Konishi, *J. Phys. Chem. A*, 2015, **119**, 4898–4906.
84 Z. Wang and J. Zhao, *Org. Lett.*, 2017, **19**, 4492–4495.
85 G. Ulrich, R. Ziessel and A. Harriman, *Angew. Chem., Int. Ed.*, 2008, **47**, 1184–1201.
86 H. Lu, J. Mack, Y. Yang and Z. Shen, *Chem. Soc. Rev.*, 2014, **43**, 4778–4823.
87 F. Tanaka and J. Osugi, *Chem. Phys. Lett.*, 1974, **27**, 133–137.
88 K. Chen, I. V. Kurganskii, X. Zhang, A. Elmali, J. Zhao, A. Karatay and M. V. Fedin, *Chem. – Eur. J.*, 2021, **27**, 7572–7587.
89 Y. Hou, T. Biskup, S. Rein, Z. Wang, L. Bussotti, N. Russo, P. Foggi, J. Zhao, M. Di Donato, G. Mazzone and S. Weber, *J. Phys. Chem. C*, 2018, **122**, 27850–27865.
90 V. Bandi, H. B. Gobeze, V. Lakshmi, M. Ravikanth and F. D'Souza, *J. Phys. Chem. C*, 2015, **119**, 8095–8102.
91 M. A. Filatov, S. Karuthedath, P. M. Polestshuk, S. Callaghan, K. J. Flanagan, M. Telitchko, T. Wiesner, F. Laquai and M. O. Senge, *Phys. Chem. Chem. Phys.*, 2018, **20**, 8016–8031.
92 M. A. Filatov, S. Karuthedath, P. M. Polestshuk, S. Callaghan, K. J. Flanagan, T. Wiesner, F. Laquai and M. O. Senge, *ChemPhotoChem*, 2018, **2**, 606–615.
93 M. Jurczok, P. Plaza, M. M. Martin, Y. H. Meyer and W. Rettig, *Chem. Phys.*, 2000, **253**, 339–349.
94 K. Xu, J. Zhao, D. Escudero, Z. Mahmood and D. Jacquemin, *J. Phys. Chem. C*, 2015, **119**, 23801–23812.
95 K. Chen, M. Hussain, S. S. Razi, Y. Hou, E. A. Yildiz, J. Zhao, H. G. Yaglioglu and M. D. Donato, *Inorg. Chem.*, 2020, **59**, 14731–14745.
96 Z. Lou, Y. Hou, K. Chen, J. Zhao, S. Ji, F. Zhong, Y. Dede and B. Dick, *J. Phys. Chem. C*, 2018, **122**, 185–193.
97 Y. Dong, A. A. Sukhanov, J. Zhao, A. Elmali, X. Li, B. Dick, A. Karatay and V. K. Voronkova, *J. Phys. Chem. C*, 2019, **123**, 22793–22811.
98 L. Huang, J. Zhao, S. Guo, C. Zhang and J. Ma, *J. Org. Chem.*, 2013, **78**, 5627–5637.
99 L. Huang, X. Cui, B. Therrien and J. Zhao, *Chem. – Eur. J.*, 2013, **19**, 17472–17482.
100 Y. Hou, Q. Liu and J. Zhao, *Chem. Commun.*, 2020, **56**, 1721–1724.
101 X. Zhang, M. Ivanov, Z. Wang, M. H. E. Bousquet, X. Liu, Y. Wan, J. Zhao, A. Barbon, D. Escudero, D. Jacquemin and M. Fedin, *Angew. Chem., Int. Ed.*, 2022, **61**, e202210419.
102 Z. Wang, A. Toffoletti, Y. Hou, J. Zhao, A. Barbon and B. Dick, *Chem. Sci.*, 2021, **12**, 2829–2840.
103 W. E. Ford and P. V. Kamat, *J. Phys. Chem.*, 1987, **91**, 6373–6380.
104 M. Montalti, A. Credi, L. Prodi and M. T. Gandolf, *Handbook of Photochemistry* CRC Press, Boca Raton, 2006.
105 T. Zhang, X. Ma and H. Tian, *Chem. Sci.*, 2020, **11**, 482–487.
106 Z. Wang, J. Zhao, M. Di Donato and G. Mazzone, *Chem. Commun.*, 2019, **55**, 1510–1513.
107 L. Franco, A. Toffoletti, M. Ruzzi, L. Montanari, C. Carati, L. Bonoldi and R. Po', *J. Phys. Chem. C*, 2013, **117**, 1554–1560.
108 S. Väth, K. Tvingstedt, A. Baumann, M. C. Heiber, A. Sperlich, J. A. Love, T.-Q. Nguyen and V. Dyakonov, *Adv. Energy Mater.*, 2017, **7**, 1602016.
109 Z. E. X. Dance, S. M. Mickley, T. M. Wilson, A. B. Ricks, A. M. Scott, M. A. Ratner and M. R. Wasielewski, *J. Phys. Chem. A*, 2008, **112**, 4194–4201.
110 S. Weber, *eMagRes*, 2017, **6**, 255–270.
111 S. Richert, C. E. Tait and C. R. Timmel, *J. Magn. Reson.*, 2017, **280**, 103–116.
112 J. W. Verhoeven, *J. Photochem. Photobiol., C*, 2006, **7**, 40–60.
113 A. Toffoletti, Z. Wang, J. Zhao, M. Tommasini and A. Barbon, *Phys. Chem. Chem. Phys.*, 2018, **20**, 20497–20503.
114 M. Imran, X. Zhang, Z. Wang, X. Chen, J. Zhao, A. Barbon and V. K. Voronkova, *Phys. Chem. Chem. Phys.*, 2021, **23**, 15835–15868.
115 F. Neese, *Wiley Interdiscip. Rev.: Comput. Mol. Sci.*, 2012, **2**, 73–78.
116 B. de Souza, G. Farias, F. Neese and R. Izsák, *J. Chem. Theory Comput.*, 2019, **15**, 1896–1904.
117 A. Baiardi, J. Bloino and V. Barone, *J. Chem. Theory Comput.*, 2013, **9**, 4097–4115.
118 B. d. Souza, F. Neese and R. Izsák, *J. Chem. Phys.*, 2018, **148**, 034104.
119 C. M. Marian, *Annu. Rev. Phys. Chem.*, 2021, **72**, 617–640.
120 E. R. Menzel, *Chem. Phys. Lett.*, 1974, **26**, 45–49.
121 A. Kirch, M. Gmelch and S. Reineke, *J. Phys. Chem. Lett.*, 2019, **10**, 310–315.
122 J. J. Snellenburg, S. Laptenok, R. Seger, K. M. Mullen, and I. H. M. Van Stokkum, *Glotaran: A Java-based graphical user interface for the R package TIMP*, 2012.
123 S. Stoll and A. Schweiger, *J. Magn. Reson.*, 2006, **178**, 42–55.
124 M. J. Frisch, G. W. Trucks, H. B. Schlegel, G. E. Scuseria, M. A. Robb, J. R. Cheeseman, i. G. Scalman, V. Barone, B. Mennucci, G. A. Petersson, H. Nakatsuji, M. Caricato, X. Li, H. P. Hratchian, A. F. Izmaylov, J. Bloino, G. Zheng, J. L. Sonnenberg, M. Hada, M. Ehara, K. Toyota, R. Fukuda, J. Hasegawa, M. Ishida, T. Nakajima, Y. Honda, O. Kitao, H. Nakai, T. Vreven, J. A. J. Montgomery, J. E. Peralta, F. Ogliaro, M. Bearpark, J. J. Heyd, E. Brothers, K. N. Kudin, V. N. Staroverov, R. Kobayashi, J. Normand, K. Raghavachari, A. Rendell, J. C. Burant, S. S. Iyengar, J. Tomasi, M. Cossi, N. Rega, M. J. Millam, M. Klene, J. E. Knox, J. B. Cross, V. Bakken, C. Adamo, J. Jaramillo, R. Gomperts, R. E. Stratmann, O. Yazyev, A. J. Austin, R. Cammi, C. Pomelli, J. W. Ochterski, R. L. Martin, K. Morokuma, V. G. Zakrzewski, G. A. Voth, P. Salvador, J. J. Dannenberg, S. Dapprich, A. D. Daniels, O. Farkas, J. B. Foresman, J. V. Ortiz, J. Cioslowski and D. J. Fox, *Gaussian 09 Revision A.01*, Gaussian, Inc., Wallingford CT, 2009.